

RESEARCH ARTICLE | DECEMBER 02 2024

## Effects of irradiation-induced voids on confined layer slips in metallic nanolaminates

Special Collection: Molecular Dynamics, Methods and Applications 60 Years after Rahman

Mahshad Fani; Luis Cervantes; Anshu Raj  ; ShuoZhi Xu  

 Check for updates

J. Chem. Phys. 161, 214702 (2024)

<https://doi.org/10.1063/5.0241799>



### Articles You May Be Interested In

Transforming underground to surface mining operation – A geotechnical perspective from case study

AIP Conference Proceedings (November 2021)

Monthly prediction of rainfall in nickel mine area with artificial neural network

AIP Conference Proceedings (November 2021)

Estimation of Karts groundwater based on geophysical methods in the Monggol Village, Saptosari District, Gunungkidul Regency

AIP Conference Proceedings (November 2021)

# Effects of irradiation-induced voids on confined layer slips in metallic nanolaminates

Cite as: J. Chem. Phys. 161, 214702 (2024); doi: 10.1063/5.0241799

Submitted: 1 October 2024 • Accepted: 14 November 2024 •

Published Online: 2 December 2024



View Online



Export Citation



CrossMark

Mahshad Fani, Luis Cervantes, Anshu Raj, and Shuozi Xu<sup>a)</sup>

## AFFILIATIONS

School of Aerospace and Mechanical Engineering, University of Oklahoma, Norman, Oklahoma 73019-1052, USA

Note: This paper is part of the JCP Special Topic on Molecular Dynamics, Methods and Applications 60 Years after Rahman.

<sup>a)</sup>Author to whom correspondence should be addressed: shuozhixu@ou.edu

## ABSTRACT

Metallic nanolaminates are promising materials for nuclear applications due to their ability to withstand extreme radiation environments by trapping irradiation-induced defects. However, the effects of irradiation-induced voids on confined layer slips (CLS) in nanolaminates remain largely unexplored. In this study, molecular dynamics simulations are employed to investigate how void size and location impact CLS in two types of Ag/Cu nanolaminates. Nanolaminated Ag and Ag single crystals are also studied as references. The results show that voids act as obstacles, significantly increasing the critical stress for dislocation glide. The void location plays a role in the critical stress but in different ways for different slip planes. The void-induced hardening is stronger on planes with lower intrinsic critical stress; as a result, adding a void homogenizes the resistance to CLS across different slip planes. Ag/Cu type II nanolaminates, where the two crystals have a “cube-on-cube” crystallographic orientation, demonstrate reduced void-induced hardening compared to type I, where two adjacent layers possess differing crystallographic orientations. In addition, some void-containing nanolaminated Ag show lower critical stress than their single-crystal line counterparts.

Published under an exclusive license by AIP Publishing. <https://doi.org/10.1063/5.0241799>

## I. INTRODUCTION

In nuclear power systems, the first wall structural materials in reactors are subject to a flux of neutrons and other radiation particles, inducing clustered defects in materials whose mechanical properties are then altered.<sup>1</sup> Metallic materials used in nuclear reactors must withstand extreme radiation environments in which irradiation can induce defects such as point defects,<sup>2</sup> interstitial<sup>3</sup> or vacancy<sup>4</sup> clusters, voids,<sup>5</sup> precipitates,<sup>6</sup> stacking fault tetrahedra,<sup>7</sup> prismatic dislocation loops of interstitial<sup>8</sup> or vacancy<sup>9</sup> types, Frank loops,<sup>10</sup> and helium bubbles.<sup>11</sup> These defects increase the yield stress while reducing the work hardening rate and ductility of materials, as well as promote the flow localization by dislocation channeling.<sup>12–14</sup> In particular, the strengthening of materials by irradiation is mainly attributed to the nucleation and aggregation of lattice defects, which act as obstacles to dislocation motion.<sup>15,16</sup> Hence, understanding irradiation-induced strengthening of metallic materials requires in-depth studies of interactions between gliding dislocations and lattice defects.

In recent years, there has been a substantial interest in employing metallic nanolaminates as irradiation-resistant materials due to

their unique structures.<sup>17</sup> These laminates consist of layers of different materials, where the interfaces between layers play a critical role in determining mechanical properties.<sup>18,19</sup> The high density of interfaces results in significant enhancements in strength, hardness, and stability, as well as desirable properties such as irradiation resistance and thermal stability.<sup>20–24</sup> The interfaces act as sinks for irradiation-induced defects, encouraging the recombination of interstitials and vacancies,<sup>25–29</sup> thereby enhancing the material's tolerance to irradiation.<sup>30</sup> In metallic nanolaminates, understanding how lattice defects such as dislocations interact with interfaces remains an important area of research. Among all dislocation gliding mechanisms in nanolaminates, the confined layer slip (CLS) operates when the layer thickness is approximately between 5 and 100 nm.<sup>17,31–33</sup> CLS occurs in nanolaminates when dislocations glide only within individual layers, not across interfaces.

Several molecular dynamics (MD) simulations have been devoted to CLS in metallic nanolaminates.<sup>34,35</sup> It has been found that the CLS process is affected by a variety of factors, including layer thickness, temperature, dislocation type, and interface structure, resulting in several different dislocation gliding modes.<sup>36–39</sup> However, no MD simulations have been performed to understand

CLS in nanolaminates with irradiation-induced voids to the best of our knowledge. In single crystals, voids are known to act as either barriers or sources of dislocations, affecting the plasticity and failure of the material.<sup>40</sup> The interactions between dislocations and voids in nanolaminates are anticipated to be more complicated due to the presence of interfaces. For example, voids were found to influence the dislocation glide forces within irradiated thin films.<sup>41</sup>

Experimentally, irradiated nanolaminates exhibit a complex relationship among dislocations, voids, and interfaces, affecting the material's properties and its radiation resistance.<sup>1</sup> In an Ag/Cu nanolaminate, for example, irradiation-induced voids were found to adhere asymmetrically across the bimetallic interfaces.<sup>42</sup> This is due to the differing surface energies and interface formation energies between these two metals.<sup>43</sup> In particular, there exists a void-free zone within 20 nm from the interface in the Cu layer, which has a higher surface energy than Ag.<sup>44</sup> This phenomenon has a great impact on the nanolaminate design. For instance, in order to increase the material's radiation tolerance, one may choose two metals with a specific difference in their surface energies, thereby manipulating the void density and location.<sup>45</sup>

The present study will focus on the Ag/Cu nanolaminates, which possess exceptional strength, electronic conductivity, thermal stability, and antibacterial properties.<sup>46–52</sup> These nanolaminates exhibit postponed plastic deformation compared to single crystal line Cu. This is more of a consequence of the lattice mismatch than it is a result of the difference in stacking fault energy between Cu and Ag.<sup>53,54</sup> An investigation into the helium-implantation of Ag/Cu nanolaminates showed that the bimetallic interfaces not only mitigated radiation damage and remained stable but also modified the defect distribution of adjacent materials as well.<sup>30</sup> However, the effects of voids on CLS in Ag/Cu nanolaminates remain unexplored. In this paper, MD simulations are performed to model the CLS process in two types of Ag/Cu nanolaminates that contain a single spherical void. Geometrical factors, including the location and size of voids, are varied. Due to the thin layer (5 nm) considered here, the void is located within the Ag layer instead of the Cu layer. To provide a reference, similar dislocation gliding processes are modeled in a nanolaminated Ag and an Ag single crystal. We will calculate the critical stress for the dislocation on different slip planes to bypass the void, as well as analyze the detailed bypass mechanism.

## II. MATERIALS AND METHODS

Atomistic simulations in this paper were performed using LAMMPS.<sup>55</sup> In this paper, all atomistic structures were analyzed and visualized using OVITO.<sup>56</sup> The embedded-atom method potential developed by Williams *et al.*<sup>57</sup> was employed for interatomic interactions.

Figure 1 shows a schematic of the simulation cell for the CLS process in the presence of a spherical void. In particular, we construct a nanolaminate by putting together two single crystalline layers, A and B. Let  $x$ ,  $y$ , and  $z$  axes represent the coordinate systems in layer A, whereas  $x'$ ,  $y'$ , and  $z'$  are the coordinate systems in layer B. The edge lengths of the simulation cell along the  $x$  (or  $x'$ ),  $y$  (or  $y'$ ), and  $z$  (or  $z'$ ) directions are fixed at 43, 10, and 26 nm, respectively. Periodic boundary conditions (PBCs) are applied along the axes of  $x$  (or  $x'$ ) and  $y$  (or  $y'$ ), while traction-free boundary conditions are implemented along the  $z$  (or  $z'$ ) axis. As a result, the

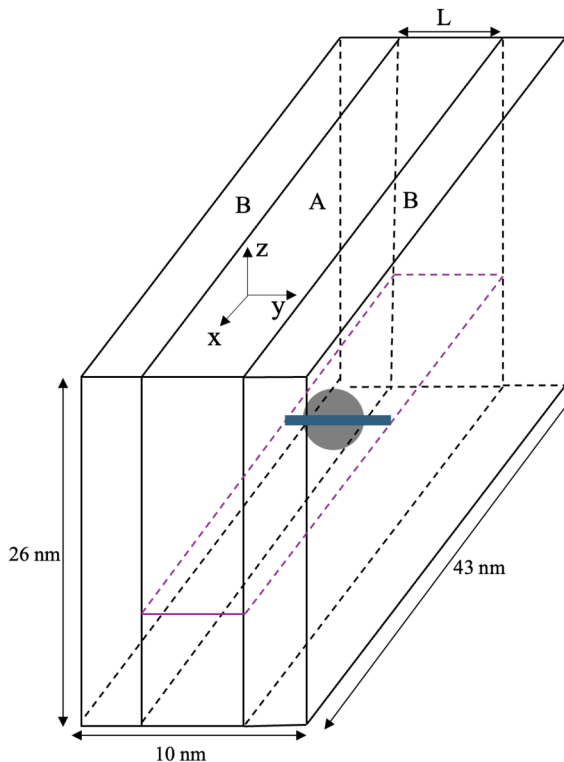


**FIG. 1.** Schematic representation of the simulation cell for CLS in nanolaminates. Two single crystalline layers, A and B, possess differing crystallographic orientations and/or materials. An edge dislocation and a spherical void are inserted into layer A.

thickness of each layer is 5 nm, the same as that used in our prior work, which studied the CLS process in void-free nanolaminates.<sup>35</sup> To find the interface with the lowest energy in each nanolaminate, layer A is shifted relative to layer B in both  $x$  and  $z$  directions to generate 100 rigid body translations. In addition, six different cutoff distances are applied, with an atom being removed from the atom pair within each distance. As a result, there are 600 initial structures for each nanolaminate. After energy minimization using the conjugate gradient algorithm, 600 interface energies are calculated and the structure with the lowest interface energy is selected.<sup>34</sup>

An edge dislocation is inserted into layer A, while layer B remains dislocation-free. As found in our prior work,<sup>35</sup> the CLS process in a void-free nanolaminate, especially the stress-strain response, is significantly affected by the specific slip plane even if they are crystallographically equivalent. For example, ten adjacent slip planes within the Ag layer in an Ag/Cu nanolaminate were found to be associated with ten different critical stresses for CLS. Here, in the void-containing nanolaminate, instead of studying all possible slip planes, we choose three representative ones, denoted as “plane<sub>max</sub>,” “plane<sub>min</sub>,” and “plane<sub>mean</sub>,” respectively. The first and second planes are those with maximum and minimum critical stresses in a void-free nanolaminate, respectively. The last plane is the one whose critical stress is the closest to the mean critical stress over the ten slip planes. Detailed positions for the three representative slip planes in different nanolaminates are shown in

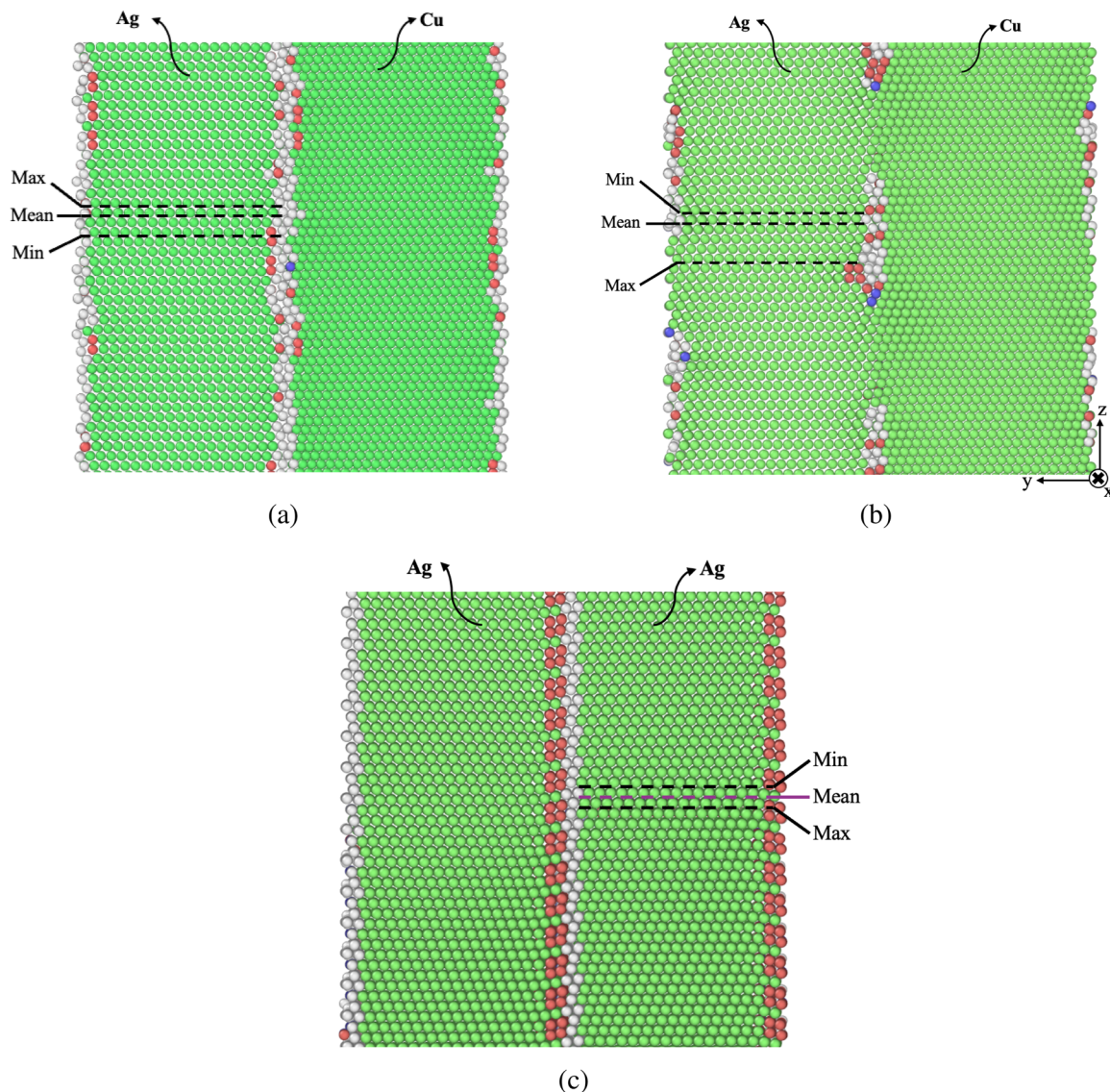


**FIG. 2.** Atomistic structures of the (a) Ag/Cu type I nanolaminate, (b) Ag/Cu type II nanolaminate, and (c) nanolaminated Ag. The green, blue, red, and gray atoms correspond to those with local FCC, BCC, HCP, and disordered lattices. The specific glide planes considered in this work, in terms of their critical stresses for void-free CLS, are marked max, mean, and min.

**Fig. 2.** In each case, adjacent to the dislocation, a spherical void is inserted by deleting atoms. Three void diameters are considered: 0.5, 1, and 2 nm. Two void locations are considered: (i) at the center of the layer A and (ii) adjacent to the interface between the layers A and B. In the second case, the void is positioned within layer A, and the distance from the interface to the void center equals the void's radius. The void locations are selected to approximate the asymmetrical adherence experimentally observed across bimetallic interfaces. In either case, no void exists in layer B, because the thickness of the void-free region, 20 nm, is larger than the layer thickness, 5 nm.

Depending on the crystallographic orientations and materials in layers A and B, we construct three types of nanolaminates, as summarized in Table I. The first type is named “Ag/Cu type I nanolaminate,” while the two layers have differing crystallographic orientations and materials. The second type is named “Ag/Cu type II nanolaminate,” while the two layers have the same crystallographic orientation but differing materials. Note that the two layers have the so-called cube-on-cube orientation. The third type is named “nanolaminated Ag” because the two layers have the same material but different crystallographic orientations. In all nanolaminates, the

**TABLE I.** Crystallographic orientations and materials in the two layers in different nanolaminates. Orientations and material in the single crystal case are also presented, whereas only layer A is involved.

	$x$	$y$	$z$	$x'$	$y'$	$z'$
Ag/Cu type I nanolaminate	[1̄10]	[112]	[1̄11]	[1̄10]	[11̄2]	[111]
Ag/Cu type II nanolaminate	[1̄10]	[11̄2]	[111]	[1̄10]	[11̄2]	[111]
Nanolaminated Ag	[1̄10]	[11̄2]	[111]	[1̄10]	[112]	[1̄11]
Ag single crystal	[1̄10]	[11̄2]	[111]	...	...	...

interfaces are incoherent with a misfit dislocation network. In particular, the symmetric incoherent twin boundary in the nanolaminated Ag exhibits a repeating arrangement of two parallel sequences, which consist of Burgers vectors  $\vec{b}_1$  and  $-2\vec{b}_1$  on each {111} plane, where  $\vec{b}_1$  is a Shockley partial dislocation.<sup>58</sup>

To provide references to nanolaminates, we study CLS processes in Ag single crystals whose size and crystallographic orientations are the same as layer A. There are two types of models. The first model, referred to as “SC-Ag,” features an infinitely long edge dislocation a result of the PBCs applied along the  $y$  axis. The second model, named “FS-Ag,” includes an edge dislocation pinned between two {112} free surfaces because of the traction-free boundary conditions applied along the  $y$  axis. In the SC-Ag model, the two void locations are equivalent; hence, only the three void diameters are considered. However, in the FS-Ag model, the two positions of the voids are not equivalent. Therefore, we examine the effects of both void location and void size, as in the nanolaminates.

### III. RESULTS AND DISCUSSION

#### A. Ag/Cu type I nanolaminate

Figure 3 presents the stress-strain curves for the CLS in plane<sub>mean</sub> in the Ag/Cu type I nanolaminate. As the strain

progresses, the stress increases and decreases multiple times. The same phenomenon is found in plane<sub>min</sub> and plane<sub>max</sub> as well.

Figure 4 illustrates the change in dislocation configuration as the strain progresses for plane<sub>min</sub>. Initially, the stress increases with strain, whereas the dislocation does not change much. Then, the dislocation starts to move, while still pinned by the interface void, right before the first peak stress of 438.28 MPa, corresponding to a strain of 0.018 57. It follows that the dislocation exits the void and the stress drops by 133.68 MPa. Similar processes are observed in 13 out of the 18 total cases (three slip planes, three void sizes, and two void locations) for the Ag/Cu type I nanolaminate.

In the remaining five cases, however, the CLS process is somewhat different. Those cases include (i) 2 nm, center void, plane<sub>min</sub>; (ii) 1 nm, interface void, plane<sub>min</sub>; (iii) 2 nm, center void, plane<sub>mean</sub>; (iv) 2 nm, interface void, plane<sub>mean</sub>; and (v) 2 nm, center void, plane<sub>max</sub>. The last case is shown in Fig. 5 to demonstrate the CLS process. Initially, the stress still increases with the strain, whereas the dislocation, on the original {111}<sub>a</sub> plane, does not change much. Then, at the first peak stress of 311.11 MPa (corresponding to a strain of 0.012 92), instead of the dislocation moving, it partially climbs to an adjacent {111} plane, denoted as {111}<sub>b</sub>. Then, the climbed part's stacking fault starts to expand with the trailing partial dislocation pinned at the void. It follows that the stress drops by 64.79 MPa to a local minimum, by which the stacking fault has propagated over the entire simulation cell. Then, the stress increases again, until the second peak stress (474.20 MPa) is reached, that is when the non-climbed part of the dislocation (on plane {111}<sub>a</sub>) exits the void; see Fig. 5(e).

In this paper, we denote the maximum stress for the dislocation to bypass the void as the critical stress for CLS. It is found that both the critical stress and the magnitude of the subsequent stress drop are associated with the void size, void location, and slip plane. As shown in Fig. 6, on the same slip plane and for the same void location, the critical stress generally increases with the void size. In most cases, the void-containing nanolaminate has a higher critical stress than the void-free one (i.e., the void diameter is zero). Notably, the void-induced increase in the critical stress is larger

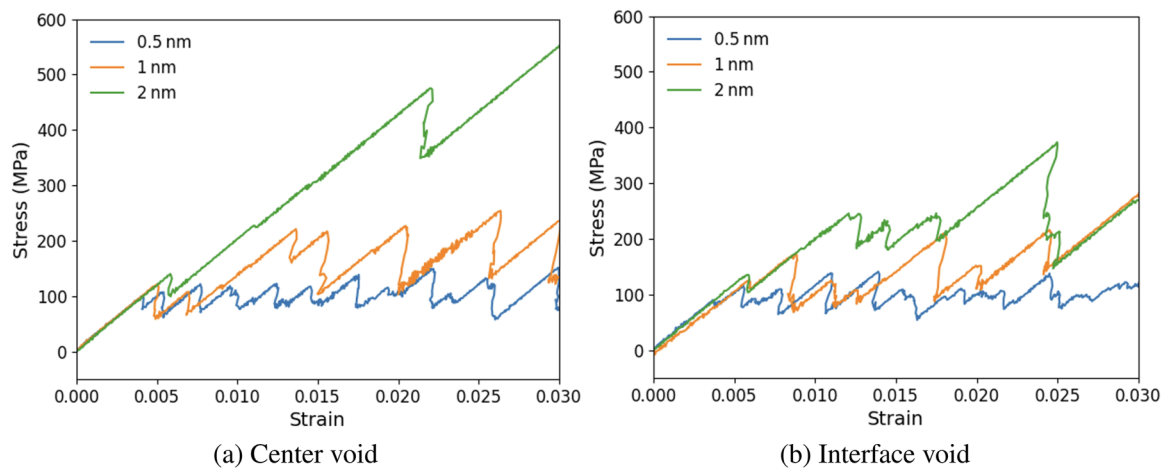


**FIG. 3.** Shear stress-strain curves for CLS within the Ag/Cu type I nanolaminate containing a void with varying diameters. The dislocation glides on plane<sub>mean</sub>. The void is either (a) at the center of the Ag layer or (b) near the interface and within the Ag layer.

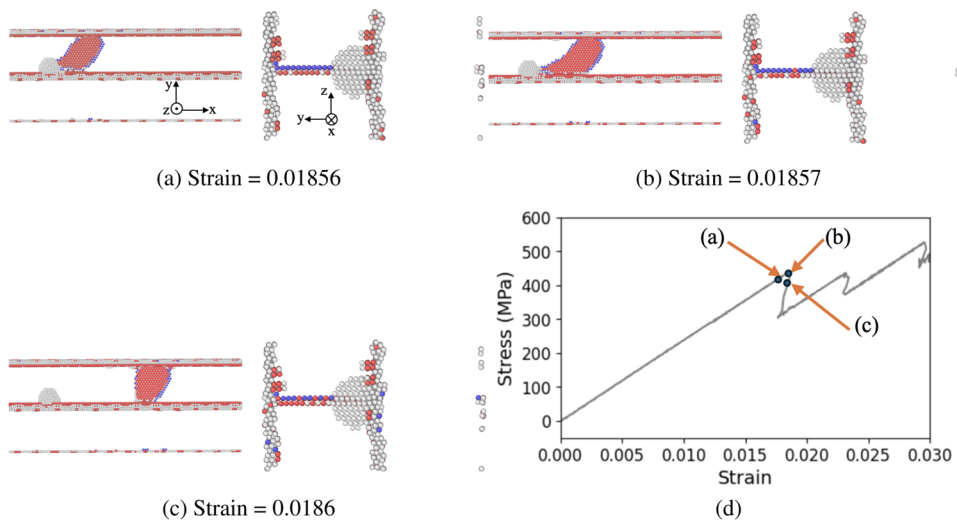


**FIG. 4.** (a)–(c) Dislocation configuration on plane<sub>min</sub> in CLS of the Ag/Cu type I nanolaminate containing an interface void with diameter being 2 nm at various shear strains. All FCC atoms are deleted, while blue represents BCCs, red represents HCPs, and gray represents disordered structures. (d) Stress-strain curve.

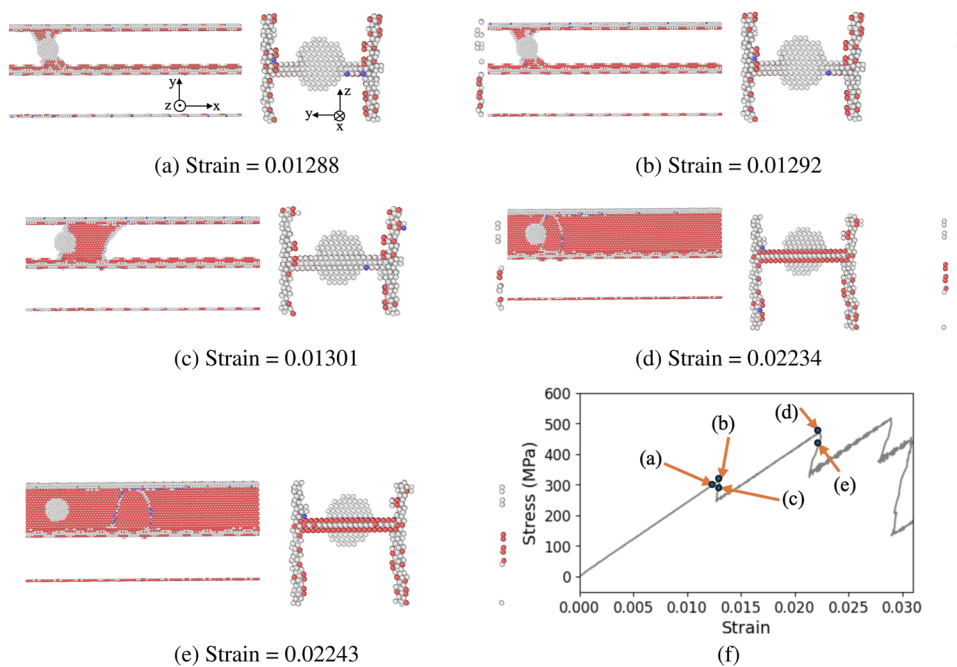


**FIG. 5.** (a)–(e) Dislocation configuration on plane<sub>max</sub> in CLS of the Ag/Cu type I nanolaminate containing a center void with the diameter being 2 nm at various shear strains. All FCC atoms are deleted, while blue represents BCCs, red represents HCPs, and gray represents disordered structures. (f) Stress-strain curve.

for plane<sub>min</sub> than for plane<sub>max</sub>. For the void location, our results show that the center void is associated with a higher critical stress than the interface void on plane<sub>max</sub>, while the opposite is true on plane<sub>min</sub>. Introducing a void at the interface appears to facilitate dislocation glide on high-resistance planes in an otherwise void-free nanolaminates. In the meantime, it makes the dislocation glide on low-resistance planes more difficult. In other words, through this redistribution of resistance, the critical stress is more uniform

or “homogenized” across the various slip planes, which results in a more consistent CLS behavior throughout the material. Taken together, our results showcase the intricacy of the void-induced hardening of nanolaminates.

### B. Ag/Cu type II nanolaminate

The stress-strain curves for the Ag/Cu type II nanolaminates are similar to those for the type I nanolaminates. Hence, the curves

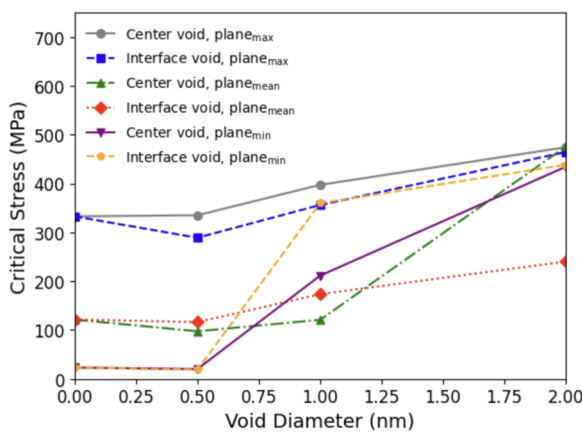


**FIG. 6.** Critical stress for CLS as a function of void diameter for different slip planes and void locations in the Ag/Cu type I nanolaminates.

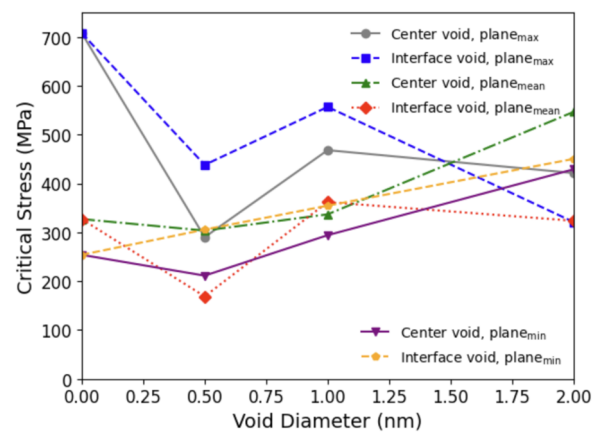


**FIG. 8.** Critical stress for CLS as a function of void diameter for different slip planes and void locations in the Ag/Cu type II nanolaminates.

are not shown here. Figure 7 shows the dislocation configurations on plane<sub>max</sub> at different shear strains. The stacking fault expands moderately before the entire dislocation exits the void. In our previous work,<sup>35</sup> we found that in a void-free type II nanolaminates, the dislocation partially climbed, forming a jog, which moves along with the dislocation as the strain increases. In the presence of a void, however, the jog is pinned by the void and does not move forward with the other parts of the dislocation; see Fig. 7(c). A similar “partial climb + pinned by the void” phenomenon was observed on plane<sub>max</sub> for all other center voids. However, the dislocation climb was subdued if the void is located at the interface. In all 18 cases for the Ag/Cu type II nanolaminates, the critical stress for the dislocation to exit the void is the first peak stress, except in the case of the CLS on plane<sub>mean</sub> in the presence of a center void with diameter being 2 nm. In that special case, the dislocation exits the void at the second peak stress, with the critical stress being 546.60 MPa.

The critical stresses for CLS in the Ag/Cu type II nanolaminates are shown in Fig. 8. Similar to the type I nanolaminates, the critical

stress is found to be a function of void size, void location, and specific slip plane. Between type I and type II nanolaminates, we found that the void-induced hardening is much less in the latter, corresponding to the fact that the void-free type II nanolaminates is more than twice as strong as the type I counterpart.

### C. Nanolaminated Ag, FS-Ag, and SC-Ag

Figures 9(a) and 9(b) present the shear stress-strain curves for CLS on the plane<sub>mean</sub> in a nanolaminated Ag. The curves are similar to those in Ag/Cu nanolaminates. Figure 9(c) shows the stress-strain responses for CLS in the FS-Ag model, where the dislocation is pinned between two traction-free surfaces. Similar to the nanolaminated Ag, the void size dependence on the critical stress is much stronger for the interface void than for the center void. Finally, Fig. 9(d) includes the stress-strain responses for CLS in the SC-Ag model, where the dislocation line is infinitely long. While the void-free SC-Ag model has a lower critical stress than the void-free FS-Ag model, the void-containing SC-Ag model has a higher critical

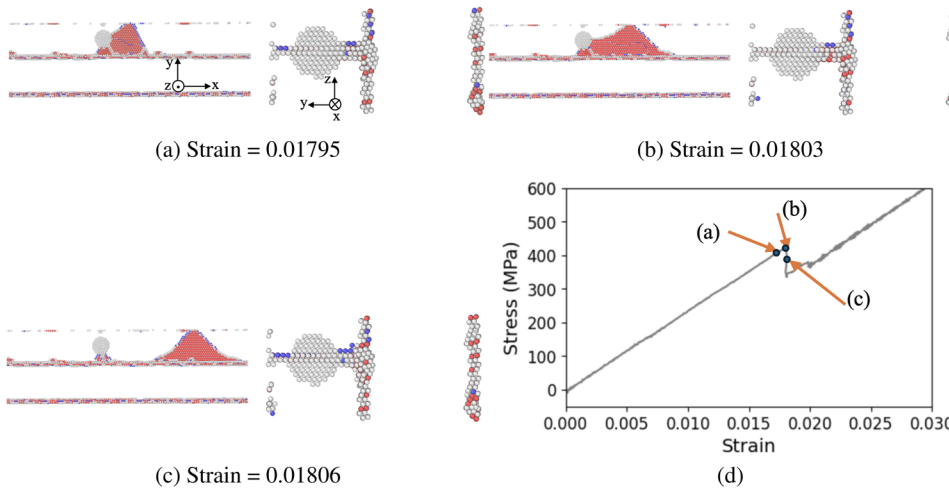


**FIG. 7.** (a)–(c) Dislocation configuration on plane<sub>max</sub> in CLS of the Ag/Cu type II nanolaminate containing a center void with diameter being 2 nm at various shear strains. All FCC atoms are deleted, while blue represents BCCs, red represents HCPs, and gray represents disordered structures. (d) Stress-strain curve.

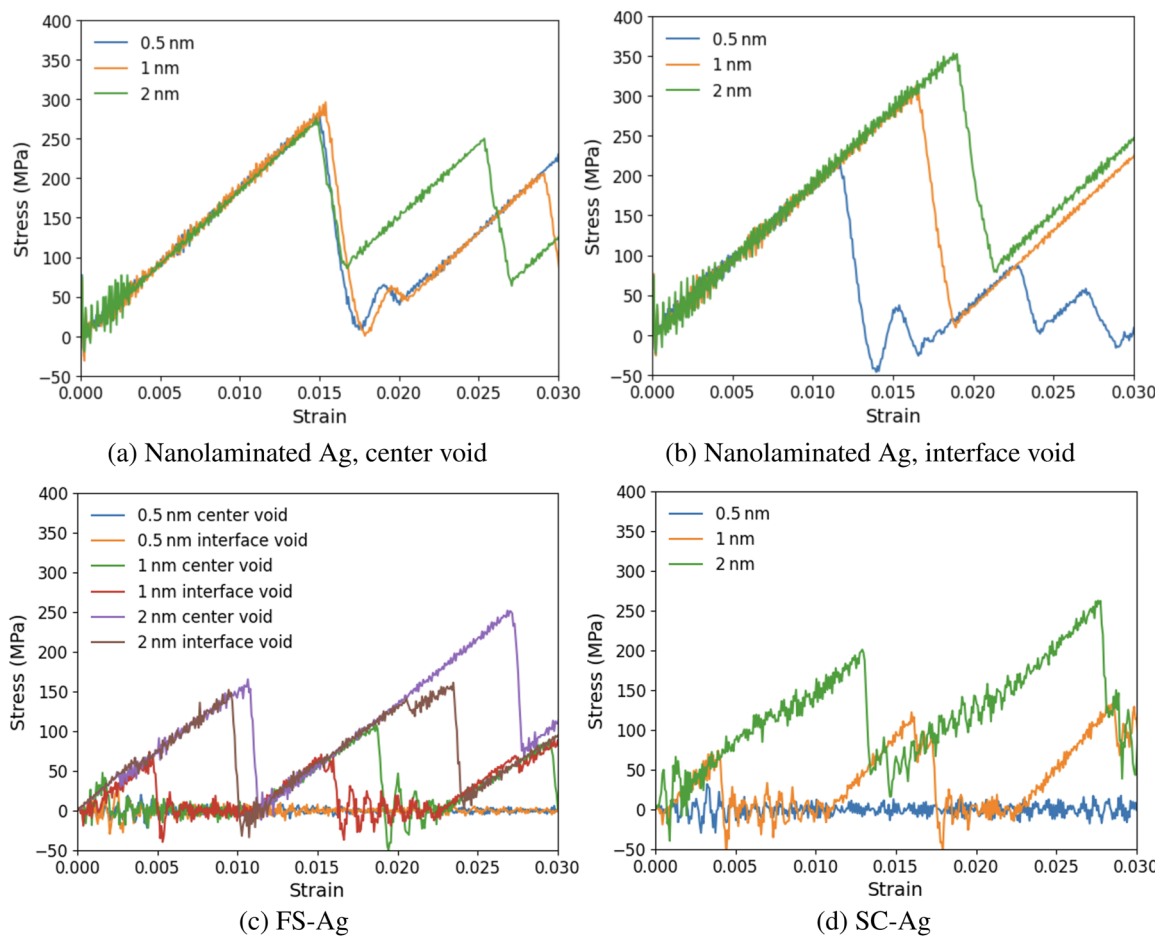


**FIG. 9.** Shear stress–strain curves for CLS within the void-containing nanolaminated Ag, FS-Ag, and SC-Ag models. In the nanolaminated Ag, the dislocation glides on  $\text{plane}_{\text{mean}}$ . The void is either (a) at the center of the layer or (b) near the interface. Panels (c) and (d) are for Ag single crystals, with (c) being the case where the dislocation is pinned between two traction-free surfaces, i.e., FS-Ag, and (d) being the case where the dislocation is infinitely long, i.e., SC-Ag.

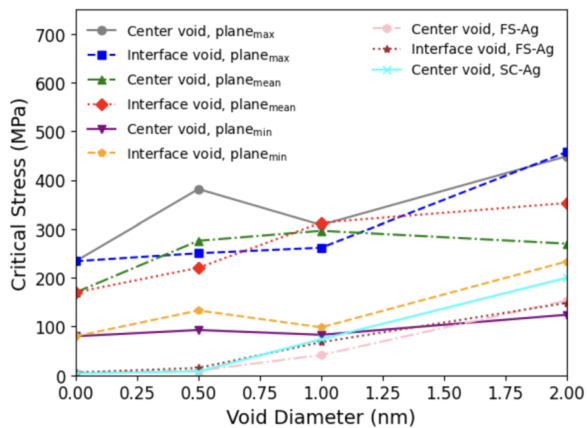


**FIG. 10.** Critical stress for CLS as a function of void diameter for different slip planes and void locations in nanolaminated Ag, FS-Ag, and SC-Ag models.

stress than its FS-Ag counterpart. This finding is likely due to that adding a void (with traction-free surface) disrupts the SC-Ag model more than the FS-Ag model, which already has two traction-free surfaces. Figure 10 shows all critical stresses for CLS in nanolaminated Ag, FS-Ag, and SC-Ag. It is shown that some void-containing nanolaminated Ag has a lower critical stress than Ag single crystals, in contrary to the void-free cases. In all cases, the dislocation gliding mode is similar to those in Fig. 4, i.e., the critical stress is the first peak stress. No dislocation climb was observed, except in the nanolaminated Ag for  $\text{plane}_{\text{max}}$  in the presence of a 1 nm void at the interface.

#### IV. CONCLUSIONS

Using MD simulations, we investigate the effects of irradiation-induced voids on CLS in two types of Ag/Cu nanolaminates, nanolaminated Ag, and two types of Ag single crystals. The results demonstrate that while voids play an important role in influencing

the stress-strain response and CLS behavior, their impacts, even in the same system, strongly depend on many factors, including the void size, void location, and specific slip plane. Our key findings are as follows:

- In Ag/Cu nanolaminates, larger voids increase the critical stress required for dislocation glide; a void near the interface reduces an originally high critical stress while decreasing an originally low critical stress.
- Dislocation glide is hindered by the presence of voids, and the stress-strain curves exhibit multiple peaks due to the complex interactions between dislocations, voids, and interfaces. In most cases, the dislocation exits the void at the first peak stress, while in some cases, it does at the second peak stress.
- Different slip planes in the same material exhibit varying critical stresses in the presence of voids. For instance, this study identifies three representative planes based on the critical stress in the void-free case—max, min, and mean—and notes that the void-induced increase in critical stress is larger for plane<sub>min</sub> than for plane<sub>max</sub>.
- Ag/Cu type II nanolaminates, where the two layers have the same crystallographic orientation but different materials, exhibit less void-induced hardening compared to type I nanolaminates. In Ag single crystals, the presence of voids increases the critical stress similarly to the nanolaminates. In certain cases, void-containing nanolaminated Ag shows lower critical stress than the single-crystal Ag models.

## ACKNOWLEDGMENTS

This work used Bridges-2 at the Pittsburgh Supercomputing Center through allocation Grant No. MAT230058 from the Advanced Cyberinfrastructure Coordination Ecosystem: Services & Support (ACCESS) program, which is supported by the National Science Foundation under Grant Nos. 2138259, 2138286, 2138307, 2137603, and 2138296. Some of the computing for this project was performed at the OU Supercomputing Center for Education & Research (OSCAR) at the University of Oklahoma (OU). This research was supported in part by a grant from the Research Council of the OU Norman Campus. M.F., A.R., and S.X. acknowledge the startup funds provided by OU.

## AUTHOR DECLARATIONS

### Conflict of Interest

The authors have no conflicts to disclose.

### Author Contributions

**Mahshad Fani:** Data curation (equal); Formal analysis (equal); Investigation (lead); Software (equal); Validation (equal); Visualization (equal); Writing – original draft (lead). **Luis Cervantes:** Data curation (equal); Formal analysis (equal); Software (equal); Validation (equal); Visualization (equal). **Anshu Raj:** Data curation

(equal); Software (equal). **Shuozhi Xu:** Conceptualization (lead); Funding acquisition (lead); Methodology (equal); Project administration (lead); Resources (equal); Supervision (lead); Validation (equal); Writing – review & editing (lead).

## DATA AVAILABILITY

The data that support the findings of this study are openly available at [https://github.com/shuozhixu/JCP\\_2024](https://github.com/shuozhixu/JCP_2024).

## REFERENCES

- D. J. Bacon and Y. N. Osetsky, *Math. Mech. Solids* **14**, 270 (2009).
- K. Miller, *J. Phys. F: Met. Phys.* **11**, 1175 (1981).
- Y. Fan, Y. N. Osetsky, S. Yip, and B. Yildiz, *Proc. Natl. Acad. Sci. U. S. A.* **110**, 17756 (2013).
- A. Calder, D. J. Bacon, A. Barashev, and Y. N. Osetsky, *Philos. Mag. Lett.* **88**, 43 (2008).
- S. Xu, Z. Hao, Y. Su, W. Hu, Y. Yu, and Q. Wan, *Radiat. Eff. Defects Solids* **167**, 12 (2012).
- A. Lehtinen, F. Granberg, L. Laurson, K. Nordlund, and M. J. Alava, *Phys. Rev. E* **93**, 013309 (2016).
- H. Fan, J. A. El-Awady, and Q. Wang, *J. Nucl. Mater.* **458**, 176 (2015).
- D. Rodney, G. Martin, and Y. Bréchet, *Mater. Sci. Eng. A* **309**, 198 (2001).
- V. Gavini, K. Bhattacharya, and M. Ortiz, *Phys. Rev. B* **76**, 180101 (2007).
- S. Hayakawa, Y. Hayashi, T. Okita, M. Itakura, K. Suzuki, and Y. Kuriyama, *Nucl. Mater. Energy* **9**, 581 (2016).
- W.-R. Jian, S. Xu, Y. Su, and I. J. Beyerlein, *Acta Mater.* **230**, 117849 (2022).
- S. J. Zinkle and K. Farrell, *J. Nucl. Mater.* **168**, 262 (1989).
- M. Victoria, N. Baluc, C. Bailat, Y. Dai, M. Lupo, R. Schaublin, and B. Singh, *J. Nucl. Mater.* **276**, 114 (2000).
- B. Singh, A. Horsewell, P. Toft, and D. Edwards, *J. Nucl. Mater.* **224**, 131 (1995).
- A. Patra and D. L. McDowell, *Philos. Mag.* **92**, 861 (2012).
- Y. Chen, K. Y. Yu, Y. Liu, S. Shao, H. Wang, M. Kirk, J. Wang, and X. Zhang, *Nat. Commun.* **6**, 7036 (2015).
- I. Beyerlein and J. Wang, *MRS Bull.* **44**, 31 (2019).
- S. Subedi, I. J. Beyerlein, R. LeSar, and A. D. Rollett, *Scr. Mater.* **145**, 132 (2018).
- J. Wang, Q. Zhou, S. Shao, and A. Misra, *Mater. Res. Lett.* **5**, 1 (2017).
- S. Pathak, N. Velisavljevic, J. K. Baldwin, M. Jain, S. Zheng, N. A. Mara, and I. J. Beyerlein, *Sci. Rep.* **7**, 8264 (2017).
- M. Nasim, Y. Li, M. Wen, and C. Wen, *J. Mater. Sci. Technol.* **50**, 215 (2020).
- M. J. Demkowicz and I. J. Beyerlein, *Scr. Mater.* **187**, 130 (2020).
- H. Gleiter, *Acta Mater.* **48**, 1 (2000).
- M. A. Meyers, A. Mishra, and D. J. Benson, *Prog. Mater. Sci.* **51**, 427 (2006).
- X. Zhang, K. Hattar, Y. Chen, L. Shao, J. Li, C. Sun, K. Yu, N. Li, M. L. Taheri, H. Wang *et al.*, *Prog. Mater. Sci.* **96**, 217 (2018).
- W. Han, M. J. Demkowicz, N. A. Mara, E. Fu, S. Sinha, A. D. Rollett, Y. Wang, J. S. Carpenter, I. J. Beyerlein, and A. Misra, *Adv. Mater.* **25**, 6975 (2013).
- M. Demkowicz, R. Hoagland, and J. Hirth, *Phys. Rev. Lett.* **100**, 136102 (2008).
- W. Han, M. Demkowicz, E. Fu, Y. Wang, and A. Misra, *Acta Mater.* **60**, 6341 (2012).
- I. Beyerlein, M. Demkowicz, A. Misra, and B. Uberuaga, *Prog. Mater. Sci.* **74**, 125 (2015).
- M. Wang, I. J. Beyerlein, J. Zhang, and W.-Z. Han, *Acta Mater.* **160**, 211 (2018).
- J. Embury and J. Hirth, *Acta Metall. Mater.* **42**, 2051 (1994).
- W. D. Nix, *Metall. Trans. A* **20**, 2217 (1989).
- I. J. Beyerlein, Z. Li, and N. A. Mara, *Annu. Rev. Mater. Res.* **52**, 281 (2022).
- W.-R. Jian, Y. Su, S. Xu, W. Ji, and I. J. Beyerlein, *J. Mater. Res.* **36**, 2802 (2021).
- M. Fani, W.-R. Jian, Y. Su, and S. Xu, *Materials* **17**, 501 (2024).
- Q. Li and P. M. Anderson, *MRS Online Proc. Libr.* **791**, 519 (2003).
- M. An, H. Song, Q. Deng, M. Su, and Y. Liu, *J. Appl. Phys.* **125**, 16 (2019).
- P. Anderson, T. Foecke, and P. Hazzledine, *MRS Bull.* **24**, 27 (1999).

- <sup>39</sup>L. Yang, C. Mayer, N. Chawla, J. Llorca, and J. Molina-Aldareguía, *Philos. Mag.* **96**, 3336 (2016).
- <sup>40</sup>L. Yuan, C. Xu, J. Xu, D. Shan, and B. Guo, *J. Mater. Eng. Perform.* **29**, 6617 (2020).
- <sup>41</sup>Y. Y. Cai, J. P. Guo, and Y. P. Chen, *Key Eng. Mater.* **725**, 189 (2016).
- <sup>42</sup>Z. Yan, Z. Liu, X. Kong, B. Yao, Q. An, S. Jiang, R. Zhang, I. J. Beyerlein, and S. Zheng, *J. Nucl. Mater.* **558**, 153380 (2022).
- <sup>43</sup>X. Kong, N. Gao, I. J. Beyerlein, B. Yao, S. Zheng, X. Ma, D. Legut, T. C. Germann, H. Zhang, and R. Zhang, *Acta Mater.* **188**, 623 (2020).
- <sup>44</sup>S. Zheng, J. Pang, L. Yang, W. Yang, Y. Zhou, Y. Wang, F. Yin, and X. Ma, *Appl. Phys. Lett.* **116**, 093703 (2020).
- <sup>45</sup>S. Zheng, S. Shao, J. Zhang, Y. Wang, M. J. Demkowicz, I. J. Beyerlein, and N. A. Mara, *Sci. Rep.* **5**, 15428 (2015).
- <sup>46</sup>Y. Wei, L. Qiao, K. Han, and L. Yang, *Physica B* **644**, 414245 (2022).
- <sup>47</sup>L. Ghalandari and M. Moshksar, *J. Alloys Compd.* **506**, 172 (2010).
- <sup>48</sup>H. Dong, Y. Chen, Y. Guo, G. Shan, G. Yang, L. Huang, F. Liu, and Q. Li, *Mater. Charact.* **196**, 112613 (2023).
- <sup>49</sup>D. Yao and L. Meng, *Physica B* **403**, 3384 (2008).
- <sup>50</sup>V. M. Villapún, L. G. Dover, A. Cross, and S. González, *Materials* **9**, 736 (2016).
- <sup>51</sup>S. Rtimi, R. Sanjines, C. Pulgarin, and J. Kiwi, *ACS Appl. Mater. Interfaces* **8**, 47 (2016).
- <sup>52</sup>R. L. Sakaguchi and J. M. Powers, *Craig's Restorative Dental Materials* (Elsevier Health Sciences, 2011).
- <sup>53</sup>A. Kardani and A. Montazeri, *Sci. Rep.* **10**, 9745 (2020).
- <sup>54</sup>Y.-Y. Tian, J. Li, Z.-Y. Hu, Z.-P. Wang, and Q.-H. Fang, *Chin. Phys. B* **26**, 126802 (2017).
- <sup>55</sup>A. P. Thompson, H. M. Aktulga, R. Berger, D. S. Bolintineanu, W. M. Brown, P. S. Crozier, P. J. in't Veld, A. Kohlmeyer, S. G. Moore, T. D. Nguyen *et al.*, *Comput. Phys. Commun.* **271**, 108171 (2022).
- <sup>56</sup>A. Stukowski, *Modell. Simul. Mater. Sci. Eng.* **18**, 015012 (2009).
- <sup>57</sup>P. Williams, Y. Mishin, and J. Hamilton, *Modell. Simul. Mater. Sci. Eng.* **14**, 817 (2006).
- <sup>58</sup>J. Wang, O. Anderoglu, J. Hirth, A. Misra, and X. Zhang, *Appl. Phys. Lett.* **95**, 021101 (2009).